# Journal Pre-proof

Developing mechanically robust, triazole-zwitterionic hydrogels to mitigate foreign body response (FBR) for islet encapsulation

Qingsheng Liu, Alan Chiu, Longhai Wang, Duo An, Wenchen Li, Esther Y. Chen, Yu Zhang, Yehudah Pardo, Sean P. McDonough, Lingyun Liu, Wendy F. Liu, Jing Chen, Minglin Ma

PII: S0142-9612(19)30739-2

DOI: https://doi.org/10.1016/j.biomaterials.2019.119640

Reference: JBMT 119640

To appear in: Biomaterials

Received Date: 29 June 2019

Revised Date: 17 November 2019 Accepted Date: 18 November 2019

Please cite this article as: Liu Q, Chiu A, Wang L, An D, Li W, Chen EY, Zhang Y, Pardo Y, McDonough SP, Liu L, Liu WF, Chen J, Ma M, Developing mechanically robust, triazole-zwitterionic hydrogels to mitigate foreign body response (FBR) for islet encapsulation, *Biomaterials* (2019), doi: https://doi.org/10.1016/j.biomaterials.2019.119640.

This is a PDF file of an article that has undergone enhancements after acceptance, such as the addition of a cover page and metadata, and formatting for readability, but it is not yet the definitive version of record. This version will undergo additional copyediting, typesetting and review before it is published in its final form, but we are providing this version to give early visibility of the article. Please note that, during the production process, errors may be discovered which could affect the content, and all legal disclaimers that apply to the journal pertain.

© 2019 Published by Elsevier Ltd.



Developing mechanically robust, triazole-zwitterionic hydrogels to mitigate foreign body response (FBR) for islet encapsulation

Authors: Qingsheng Liu<sup>1</sup>, Alan Chiu<sup>1</sup>, Longhai Wang<sup>1</sup>, Duo An<sup>1</sup>, Wenchen Li<sup>2</sup>, Esther Y. Chen<sup>3</sup>, Yu Zhang<sup>1</sup>, Yehudah Pardo<sup>1</sup>, Sean P. McDonough<sup>4</sup>, Lingyun Liu<sup>2</sup>, Wendy F. Liu<sup>3</sup>, Jing Chen<sup>1</sup>, Minglin Ma<sup>1</sup>,\*

<sup>&</sup>lt;sup>1</sup> Department of Biological and Environmental Engineering, Cornell University, Ithaca, New York 14853, USA

<sup>&</sup>lt;sup>2</sup> Department of Chemical and Biomolecular Engineering, The University of Akron, Akron, Ohio 44325, USA

<sup>&</sup>lt;sup>3</sup> Department of Biomedical Engineering, University of California Irvine, Irvine, CA 92697, USA

<sup>&</sup>lt;sup>4</sup> Department of Biomedical Sciences, Cornell University, Ithaca, New York 14853, USA

<sup>\*</sup>To whom correspondence should be addressed. Email: mm826@cornell.edu.

#### **Abstract**

Zwitterionic hydrogels such as those based on polycarboxybetaine (PCB) or polysulfobetaine (PSB) have potential for various biomedical applications, due to their biocompatibility and low biofouling properties. However, the poor mechanical properties of zwitterionic hydrogels developed to date remain a challenge, severely limiting their practical uses. To improve the mechanical properties without compromising their zwitterionic feature or biocompatibility, we designed a new class of zwitterionic hydrogels by introducing triazole moieties into the hydrogel monomers that could form energy-dissipating  $\pi$ - $\pi$  stacking. Compared to conventional zwitterionic hydrogels, the triazole-zwitterionic (TR-ZW) ones exhibited similarly excellent antifouling properties, but were much more mechanically robust with higher stretchability (250 % tensile strain), better compression-resistance (89% compressive strain and 65% compression for at least 10 cycles without any crack) and better folding-resistance. In addition, upon subcutaneous implantation in mice, the TR-ZW hydrogels induced significantly lower foreign body responses (FBR) (i.e. less fibrosis and more blood vessel formation relative to a poly(2-hydroxyethyl methacrylate) hydrogel control). As an example for their potential applications, we showed the use of the TR-ZW hydrogels for islet encapsulation and transplantation and demonstrated diabetes correction up to ~1 month in mice in the convenient subcutaneous site

**Keywords:** tough triazole-zwitterionic hydrogels; foreign body response; vascularization; islet transplantation; type 1 diabetes.

### 1. Introduction

Hydrogel materials have received extensive interest for biomedical applications including tissue engineering [1], cell or drug delivery [2, 3], and medical devices [4, 5]. However, the performance of implanted hydrogels is often impeded by the foreign body response (FBR), which results in host recognition and subsequent formation of a dense, avascular collagenous capsule [6, 7]. This capsule compromises the diffusion of analytes, oxygen and nutrients, contributing to the implant failure. In fact, the FBR occurs for almost all implants and represents a major challenge and a difficult problem to overcome in the biomedical research and clinics. For example, poly(ethylene glycol) (PEG) and their derivative hydrogels are considered among the most biocompatible materials and have been widely used for biomedical applications [8]. However, conventional PEG hydrogels, whose biocompatibility is indeed sufficient in many cases, can still induce FBR and fibrosis upon implantation [9]. In addition, PEG is susceptible to oxidative degradation, especially in the presence of oxygen and transition metal ions, limiting their long-term applications [10]. Thus, there is a critical need to develop novel biomaterials and medical devices that can mitigate the FBR [3, 11, 12].

Nonspecific protein adsorption on the implant surfaces is considered the first, critical step in triggering a FBR [6]. Therefore, developing an antifouling material or surface that highly resists protein adsorption and cell attachment, is considered an attractive approach to mitigating a FBR. In the past few years, zwitterionic polymers and hydrogels, bearing zwitterions of carboxybetaine, sulfobetaine or phosphorycholine, have drawn tremendous attention as a result of their ultra-low-fouling properties [13-19]. For example, zwitterionic poly(carboxybetaine methacrylate) (PCB) hydrogel was shown to resist the FBR (i.e. with low fibrosis and high vascularization) after 3 months of subcutaneous implantation in mice [20]. Given the increasing

interest in implantable devices, this result was considered a breakthrough in biomedical research [21]. However, there exists a significant challenge: the PCB hydrogel as well as other pure zwitterionic hydrogels developed to date, tend to have unsatisfactory mechanical properties such as weakness or brittleness, limiting the scope of their applications [22, 23].

In principle, the mechanical properties of zwitterionic hydrogels may be improved by blending zwitterionic polymers with a different polymer or copolymerizing with a different monomer [24-26]. Unfortunately, those approaches tend to compromise zwitterionic features or FBR-resistant properties of the material. Long-term mechanical robustness, exceptional antifouling properties, and excellent FBR-resistant characteristics do not coexist in existing pure zwitterionic hydrogels. To address this issue, we designed a new class of zwitterionic hydrogels in which we integrated triazole and zwitterionic moieties into a same monomer. The rationales of incorporating triazole groups are two folds. First, it was recently discovered by Vegas et al. through a high throughput combinatorial screening that chemically modified alginate hydrogels containing triazole groups were capable of mitigating the fibrotic response in primates for 6 months [27, 28]. The distribution of the triazole modification created a unique hydrogel surface that resisted macrophage recognition and fibrosis formation. Second, the triazole rings can form reversible  $\pi$ - $\pi$  stacking [29, 30] that can improve the mechanical strength of hydrogels through an energy-dissipation mechanism [31]. In addition, quaternization (e.g. by methylation) of the nitrogen at N1 in the triazole ring leads to a permanent positive charge, naturally serving as the cationic component of the zwitterionic monomer.

In this work, we first synthesized and characterized a poly (quaternized triazole carboxybetaine acrylamide) hydrogel, termed as P(qTR-CB). Similar to the PCB hydrogel reported previously [13], the P(qTR-CB) hydrogel exhibited remarkably low non-specific protein

adsorption. However, the P(qTR-CB) hydrogel was shown much more mechanically robust. Further *in vitro* experiment showed that the P(qTR-CB) hydrogel also had low non-specific cell attachment and macrophage activation. Encouraged by these results, we then synthesized two additional triazole-zwitterionic (TR-ZW) hydrogels: poly(triazole carboxybetaine acrylamide) or P(TR-CB) (i.e. without quaternization of the triazole group) and poly(triazole sulfobetaine acrylamide) or P(TR-SB). Upon subcutaneous implantation in immunocompetent mice, all the TR-ZW hydrogels induced less fibrosis and promoted more blood vessel formation when compared to a poly(2-hydroxyethyl methacrylate) (PHEMA) hydrogel control. Notably, the P(TR-SB) was shown much more resilient and seemed to be similar or even more FBR-resistant than other TR-ZW hydrogels or previously reported PCB hydrogel [20]. We further showed the potential use of the P(TR-SB) hydrogel for islet encapsulation to treat type 1 diabetes (T1D). Upon subcutaneous transplantation in immunocompetent, chemically induced diabetic mice, the P(TR-SB) hydrogel encapsulating rat islets enabled better diabetes correction than a conventional alginate hydrogel control with similar doses of islets.

## 2. Materials and Method

# 2.1. Materials/Reagents

Propargylamine, acryloyl chloride, sodium azide, sodium ascorbate, copper sulfate pentahydrate, iodomethane, trifluoroacetic acid (TFA), 2-chloro-*N*, *N*-dimethylethylamine hydrochloride, 1, 3-propanesultone, 2-hydroxyethyl methacrylate (HEMA), lithium phenyl-2, 4, 6-trimethylbenzoylphosphinate (LAP), phosphate buffered saline (PBS), dichloromethane (DCM), dimethyl sulfoxide (DMSO), acetonitrile, hexane, ethyl acetate, diethyl ether, and ethyl alcohol were purchased from Sigma-Aldrich. *Tert-butyl* bromoacetate and ion exchange resin (Amberlyst A-26, OH form) were obtained from Alfa Aesar. Carboxybetaine methacrylate (CB)

[32] and carboxybetaine diacrylamide (CBAAX) [33] were synthesized using methods reported previously. Rabbit anti-insulin antibodies (Cat. #ab63820) was purchased from Abcam. Anti-Glucagon antibody (Cat. #SAB4200685) produced in mouse was purchased from Sigma-Aldrich. Alexa Fluor<sup>TM</sup> 594 donkey anti-rabbit antibody (Cat. #A-21207), Alexa Fluor<sup>TM</sup> 488 goat anti-mouse antibody (Cat. #A-11001), and Alexa Fluor<sup>TM</sup> 488 donkey anti-goat antibody (Cat. #A11055), were purchased from Invitrogen. Goat anti-mouse CD31 (Cat. # AF3628) was purchased from R&D systems. LIVE/DEAD assay kit (Cat. # L3224) was purchased form Invitrogen. The customized PDMS mold (~6.5 mm in diameter and ~1 mm depth) was fabricated using a commercial PDMS kit (Dow Corning). A pre-calculated volume of degassed PDMS presolution was cast on a petri dish and after curing, the PDMS slab was punched using a biopsy punch of 6 mm into the mold and sterilized for future use.

# 2.2. Synthesis of triazole-zwitterionic monomers

The synthesis procedures of quaternized triazole carboxybetaine acrylamide (qTR-CB), triazole carboxybetaine acrylamide (TR-CB), and triazole sulfobetaine acrylamide (TR-SB) were described in the Supporting Information.

## 2.3. Hydrogel preparation

TR-ZW hydrogels were prepared through radical polymerization initiated by UV irradiation. The hydrogel solution contains the monomer (2 M), CBAAX cross linker (0.1 M) and lithium phenyl-2, 4, 6-trimethylbenzoylphosphinate (LAP) photo-initiator (1.0 wt%, mass percent of monomer). The resulting solution was filtered through a 0.22 µm sterile filter and then cast between a pair of glass slides, separated with a 1 or 2-mm-thickness poly(tetrafluoroethylene) (PTFE) spacer, and polymerized under UV light (Omnicure S2000, 365 nm) for 10 min.

PHEMA and PCB hydrogels were prepared using a similar procedure. After preparation, all hydrogel samples were equilibrated in sterile PBS buffer and the PBS buffer solution was changed at least three times a day for 3 days. For implantation, the hydrogels were punched into disks with a diameter of 6 mm and stored in sterile PBS at 4°C before use.

## 2.4. Hydrogel tensile and compression tests

Tensile tests of hydrogel samples were performed on a TA instruments DMA Q800 Dynamic Mechanical Thermal Analysis (DMTA). All equilibrated hydrogel samples were cut in a rectangular shape with 25 mm length, 6 mm width, and 2-3 mm thickness. Hydrogel samples were stretched until failure at a rate of 5 mm/min. The compression tests and loading-unloading tests of hydrogel samples were performed on an Instron 5965 with a 100 N load cell. For compression tests, each hydrogel disk with a diameter of 6 mm (about 2-3 mm thickness when equilibrated in PBS buffer) was compressed until failure at a rate of 1 mm/min. The shape recovery property of the hydrogels was evaluated by ten consecutive loading and unloading cycles at a constant rate of 1 mm/min in the strain range of 0–65%. All samples were measured at room temperature.

## 2.5. Protein adsorption assay

P(qTR-CB) polymer brushes were grafted onto gold-coated surface plasmonic resonance (SPR) sensor chips following the procedure reported previously [34]. The protein adsorption on the P(qTR-CB)-grafted gold surfaces was evaluated using a four-channel SPR sensor. Firstly, PBS buffer was flowed into the channels for 10 min to build the baseline. Secondly, a 1 mg/mL fibrinogen solution or 100% human blood plasma was run through the channels for 10 min followed by a PBS buffer wash to remove unbound protein molecules. The amount of adsorbed

protein was finally quantified by the change of wavelength shift between the pre-adsorptive and post-adsorptive baselines. A 1 nm SPR wavelength shift at 750 nm corresponded to a protein surface coverage of 15 ng/cm<sup>2</sup> [32]. The amount of protein adsorption on the P(TR-CB) and P(TR-SB) surfaces was evaluated using the same procedure.

## 2.6. Cell attachment assay

NIH/3T3 cells were cultured in a humidified incubator with 5% CO<sub>2</sub> at 37°C before use. The culture medium was composed of Dulbecco's modified Eagle medium (DMEM), 10% fetal bovine serum (FBS), and 2% penicillin streptomycin. The hydrogel disks with a diameter of 6 mm were individually placed into a 12-well plate and washed with sterile PBS buffer three times. 2 mL of cell suspension (concentration: 10<sup>5</sup> cells/mL) was then transferred into each well and incubated with these hydrogels for 3 days at 37°C. After incubation, the hydrogels were transferred to a new 12-well plate containing sterile PBS in each well. The LIVE/DEAD assay kit was added into each well and incubated for 30 min. These hydrogels were finally imaged by using an EVOS AMF4300 imaging system.

# 2.7. Macrophage activation on the P(qTR-CB) hydrogels

All protocols involving animals were approved by the Institutional Animal Care and Use Committee at the University of California Irvine prior to initiation of the study. Bone marrow derived macrophages (BMDM) were harvested from the femurs or tibia of 6-8 week-old C57BL/6J mice (Jackson Laboratories). Cells were treated with ACK lysis buffer (Invitrogen), centrifuged, and resuspended in D-10 media, which consists of Dulbecco's modified Eagle medium (DMEM) supplemented with 2 mM L-glutamine, 100 units per mL penicillin—streptomycin, 10% heat-inactivated FBS, and 10% media collected from the supernatant of CMG

12–14 cells ectopically expressing recombinant mouse macrophage colony stimulating factor (M-CSF) [35]. BMDM were cultured at 37°C in a humidified incubator with 5% CO<sub>2</sub>. BMDM were dissociated using cell dissociation buffer (Invitrogen) on day 7, and seeded on the tissue culture plates (Olympus Plastics) or various hydrogel surfaces at a cell density of 10<sup>6</sup> cells/cm<sup>2</sup> and stimulated with different combinations: 0.3 ng/mL lipopolysaccharide (LPS) (Sigma-Aldrich), 1.0 ng/mL IFNγ (R&D systems, Minneapolis, MN), 20 ng/mL IL-4 (Invitrogen) and 20 ng/mL IL-13 (Invitrogen). After stimulation for 36 h, supernatants were collected and analyzed for TNF-α and IL-10 secretion by ELISA (enzyme-linked immunosorbent assay) following the manufacturer's instructions (BioLegend, San Diego, CA).

## 2.8. Rat islet isolation, purification and encapsulation

Male Sprague-Dawley rats from Charles River Laboratories weighing about 300 g were used for harvesting islets. All rats were anesthetized using 3% isoflurane in oxygen throughout the whole procedure. Isolation surgeries were performed following Lacy and Kostianovsky [36]. Briefly, the portal vein was clamped and rat bile duct was cannulated. The pancreas was distended by an in vivo injection of cold 0.15% Liberase (Research Grade, Sigma-Aldrich) in RPMI 1640 media solution. The perfused pancreatic organs were removed and put into 50 mL conical tubes on ice until the end of all surgeries. All the tubes containing the pancreas were then placed into in a 37°C water bath for a 29 min digestion. After that, the digestion was quenched by adding cold M199 media containing 10% heat-inactivated fetal bovine serum (HIFBS) and lightly shaking. Digested pancreases were washed twice by the same aforementioned M199 media, filtered through a 450 mm sieve, and then suspended in a Histopaque 1077 (Sigma)/M199 media gradient and centrifuged at 1700 RCF at 4°C. This gradient centrifugation step was repeated for higher purity islets. Finally, these islets were further isolated by a series of six

gravity sedimentations, in which each supernatant was discarded after 4 min of settling. Purified islets were handpicked under the microscope and washed by sterile saline solution. Islets were then cultured overnight in RPMI 1640 media with 10% HIFBS and 1% penicillin/streptomycin for further use.

Islet encapsulation into the P(TR-SB) hydrogels: the precursor gel solution was prepared in the PBS buffer as mentioned in the section of P(TR-SB) hydrogel preparation and then filtered through a 0.22 μm sterile filter. In order to minimize cell damage from the free radicals, the precursor gel solution was firstly irradiated by UV light for 5 seconds to obtain the prepolymerized solution. Then, about 500 islets were mixed into the prepolymerized solution. The solution containing islets was immediately placed into customized PDMS mold (~6.5 mm in diameter and ~1 mm thickness) and allowed to polymerize in a UV cross-linking oven for 20 seconds. The cell-encapsulating P(TR-SB) hydrogel disks were equilibrated in corresponding cell culture medium at 37°C. During the first 3-hour equilibration, the cell media was refreshed every 30 min. Finally, the P(TR-SB) hydrogels with encapsulated islets were cultured for 4 h at 37°C prior to implantation. Since the rat islets had variable sizes (50-300 μm) and there was an inevitable loss of islets during the process of encapsulation, the total number of encapsulated islets was converted into islet equivalents (IEQ, normalized to 150 μm size) [37].

Islet encapsulation into the alginate hydrogels: about 500 IEQ islets were re-suspended in a 2 % SLG100 alginate solution. The alginate solution containing islets were transferred into customized PDMS mold (~6.5 mm in diameter and ~1 mm thickness) and crosslinked using a 20 mM BaCl<sub>2</sub> gelling solution. After crosslinking, alginate disks with encapsulated islets were immediately washed 5 times with saline solution to remove residual BaCl<sub>2</sub> gelling solution,

transferred into corresponding cell culture medium, and cultured for 4 h at 37°C prior to implantation.

## 2.9. Cell viability Assay

The viability of encapsulated rat islets was examined using the live/dead assay following the manufacturer's instruction (Invitrogen). The encapsulated islets were stained with calcein AM and ethidium for 30 min at 37 °C in the dark. These samples were gently rinsed with PBS three times, and fluorescence images were captured using an EVOS AMF4300 imaging system.

## 2.10. Blood glucose monitoring

Starting post-transplantation, a small drop of blood was collected from the tail vein of each mouse using a lancet and tested using a commercial glucometer (Contour Next EZ Blood Glucose Meter), approximately two times a week. Mice with unfasted glucose levels below 200 mg/dL were considered normoglycemic.

# 2.11. Intraperitoneal glucose tolerance test (IPGTT) assay

Prior to retrieval, glucose tolerance tests were performed to assess metabolic capacity. Mice were fasted overnight before an intraperitoneal injection of glucose solution (2 g of glucose per 1 kg of body mass). Blood glucose levels were monitored at predetermined timepoints (0, 15, 30, 45, 60, 90, and 120 min) after injection.

## 2.12. Static glucose-stimulated insulin secretion (GSIS) assay

Krebs Ringer Bicarbonate (KRB) buffer [98.5 mM NaCl, 4.9 mM KCl, 2.6 mM CaCl<sub>2</sub>, 1.2 mM MgSO<sub>4</sub>·7H<sub>2</sub>O, 1.2 mM KH<sub>2</sub>PO<sub>4</sub> and 25.9 mM NaHCO<sub>3</sub> (all from Sigma-Aldrich)

supplemented with 20 mM HEPES and 0.1% BSA (Serological)] was prepared beforehand. Encapsulated islets were then incubated for 60 min in KRB buffer with 2.8 mM or 16.7 mM d-glucose under the same condition. The supernatants were collected, and insulin content was quantified using ultrasensitive mouse/rat insulin ELISA kit (ALPCO) with measurement by Synergy 4 Fluorescence Absorbance Microplate Reader (BioTek) at 450 nm wavelengths. All the ELISA results were normalized to the IEQ.

# 2.13. Mouse blood vessel perfusion

To image whether implanted hydrogels induced vessels that were connected to the mouse vasculature, mice were perfused with lipophilic carbocyanine dye DiI as previously described [38]. Briefly, a butterfly needle was inserted into left ventricle of the mouse, and 2 mL of PBS, 10 mL of DiI solution, and 10 mL of 4% (v/v) paraformaldehyde solution were perfused sequentially at the speed of 2 mL/min using a syringe pump. Immediately after perfusion, hydrogels were retrieved and imaged using laser scanning confocal microscope.

# 2.14. Hydrogel implantation, retrieval, and histological analysis

All animal protocols were approved by the Cornell Institutional Animal Care and Use Committee. Eight-week-old, immune-competent male C57BL/6 mice were obtained from Jackson Laboratory. The equilibrated hydrogel disks were implanted subcutaneously in mice for 1, 2, and 3 months, respectively. For each mouse, hydrogel disks made from different monomers were implanted on the back of the mouse and the sites of various hydrogel samples were alternated in order to eliminate the effect of implantation positions. At the end of each experiment, mice were euthanized by CO<sub>2</sub> asphyxiation. The retrieved hydrogel disks together with surrounding tissues were dissected and fixed in 10% neutrally buffered formalin. After

embedded in paraffin wax, the samples were sectioned and stained with Masson's trichrome by the Cornell Histology Core Facility.

To assess the fibrosis formation upon the hydrogel, the Masson's trichrome staining histology slides were scanned using an Aperio CS2 ScanScope (Leica Biosystems, Nusslock GmbH). The blue-pixel density was measured using Image J software. The collagen density was quantified as a percentage of average maximum blue-pixel density from all analyzed sections. For each sample, three random fields were analyzed for each fixed distance (e.g. 0 to 10  $\mu$ m; 10 to 20  $\mu$ m; etc.) within 60  $\mu$ m from the tissue-hydrogel interface. The sample size is n = 5.

To assess the blood vessel formation upon the hydrogels, paraffin-embedded sections were rehydrated by sequential washing in xylene, 100%, 95%, 75% ethanol and DI water. These slides were then boiled in 1mM EDTA for antigen exposure. Non-specific binding was blocked with 10% goat serum for 45 min at room temperature. The slides were stained using primary Goat antimouse CD31 (R&D Systems, dilution 1:200), which is an endothelial cell biomarker. Alexa Fluor 488 donkey anti-Goat as secondary antibody (Invitrogen, dilution 1:500) was employed in this work. Two stained sections at different positions of each hydrogel disks were used and five different fields were randomly examined in each section. The density of blood vessels was quantified by counting the number of the vascular features normalized to the total area. The sample size is n=5.

To conduct immunofluorescence staining of retrieved islets, the histological slides were rehydrated by sequential washing in xylene, 100%, 90%, and 75% ethanol, and DI water. These slides were then boiled in 1mM EDTA for antigen exposure. Non-specific binding was blocked with 10% goat serum for 45 min at room temperature. After blocking, slides were decanted and incubated with primary rabbit anti-insulin antibodies (1:200) overnight at 4°C. The sections were

then washed and incubated with the FITC-conjugated secondary antibodies, Alexa Fluor 594 donkey anti-rabbit antibody (1:400 dilution) for 30 min at room temperature. Slides were washed twice with water, labeled with DAPI, and covered with coverslips. Fluorescence images were captured using an EVOS AMF4300 imaging system.

## 2.15. Statistical analysis

Data are expressed as Mean  $\pm$  SEM in these experiments. Paired Student's t-test was used to compare two small sets of quantitative data from macrophage activation studies, studies of FBR to various hydrogels, studies of hydrogel modulus, and *ex vivo* GSIS experiments, with P < 0.05 being considered as statistically significant.

### 3. Results and Discussion

## 3.1. Design and mechanical characterization of the P(qTR-CB) hydrogel

In this work, we designed a new zwitterionic monomer qTR-CB (Fig. 1A) that included a triazole moiety that was previously shown to play a critical role in the anti-fibrotic properties of modified alginates[27, 28] and was known to form energy-dissipating  $\pi$ - $\pi$  stacking [29, 30, 39, 40]. As shown in Fig. 1A, the synthesis of qTR-CB monomer involved several steps: first, *N*-propargylacrylamide with dual reactive alkyne and vinyl groups was developed; the alkyne group was then transformed into triazole group through Azide-Alkyne Huisgen Cycloaddition chemistry followed by a subsequent quaternization; finally the qTR-CB monomer was obtained after removal of the protecting group of the carboxylic acid. The chemical structure of the qTR-CB monomer was confirmed by NMR (Supporting Information). We then prepared the P(qTR-CB) hydrogel by crosslinking the qTR-CB monomer with a bifunctional zwitterionic carboxybetaine diacrylamide cross-linker (CBAAX) via a photo-initiated polymerization.

The P(qTR-CB) hydrogel was designed to address the issue of poor mechanical properties displayed by current zwitterionic hydrogels which are known to be relatively brittle or weak [22, 41, 42]. Robust mechanical properties are highly desirable for handling, implantation and any future clinical applications [43]. We hypothesized that the hydrophobic interaction and reversible  $\pi$ - $\pi$  stacking between the triazole rings within the P(qTR-CB) hydrogel (Fig. 1B) could dissipate energy under load and therefore make the hydrogel more resilient. To test this hypothesis and determine whether the incorporation of the triazole rings indeed improved the mechanical property, we compared the P(qTR-CB) and conventional PCB hydrogels in several mechanical tests. First, we qualitatively examined their fold-resistance property. As shown in Fig. 1C, the P(qTR-CB) hydrogel could be completely folded close to 180 degree without fracturing or any damage, and was even amenable to repeated folding (Supplementary Movie 1). In contrast, the conventional PCB hydrogel fractured even with a small-angle folding (Fig. 1C). We then performed more quantitative tensile and compression tests. For the tensile test, the P(qTR-CB) hydrogel had a breaking strain close to 71% while the PCB hydrogel could only be stretched 11% (Fig. 1D). This represents a 6.5-fold increase in the breaking strain. For the compressive test (Fig. 1E), the P(qTR-CB) hydrogel sustained a 80% compression while the PCB hydrogel could only be compressed 48%, which was in agreement with previous work [22]. To further demonstrate the resilience of the P(qTR-CB) hydrogel, we performed a compressive loading-unloading test. As shown in Fig. 1F, the P(qTR-CB) hydrogel tolerated 65% compression for at least 10 cycles without any crack and maintained its original shape. The hysteresis loop observed in each cycle seemed to suggest that there was an energy dissipation mechanism probably due to the  $\pi$ - $\pi$ stacking between the triazole groups. This  $\pi$ - $\pi$  stacking can prevents polymer chains from sliding out of place and thereby increases the resistance to mechanical deformation [44]. To

overcome this resistance, part of the stress applied to stretch or compress the hydrogel is dissipated.

## 3.2. In vitro characterization of the P(qTR-CB) hydrogel.

Non-specific protein adsorption on the implant surface is considered the initial, critical step in the foreign body response [6]. To determine whether the qTR-CB material was anti-biofouling and resistant to non-specific protein adsorption, we grafted a gold surface with P(qTR-CB) using a surface-initiated photoiniferter-mediated polymerization [34]. The protein-resistance of P(qTR-CB) was evaluated via surface plasmon resonance (SPR) using a single protein solution and undiluted human plasma. Fig. 2A shows the typical SPR sensorgrams of protein adsorption on the P(qTR-CB)-grafted and bare gold surfaces. From a 1 mg/mL fibringen (Fg) solution, the bare gold and P(qTR-CB)-grafted surfaces had adsorptions of 337.5  $\pm$  36.1 and 0.6  $\pm$  0.3 ng/cm<sup>2</sup>, respectively. From undiluted human plasma, the amount of protein adsorptions was  $211.6 \pm 10.3$ and  $3.1 \pm 1.8 \text{ ng/cm}^2$  respectively for these two surfaces. Clearly, the P(qTR-CB)-grafted surface was highly resistant to non-specific protein adsorption, as compared to the bare gold surface. It should be noted that protein adsorption values on the P(qTR-CB)-grafted surfaces were well below the criteria for ultralow-fouling materials (less than 5 ng/cm<sup>2</sup> adsorbed fibrinogen) [45]. These data suggest that incorporation of triazole group did not compromise the zwitterionic or anti-fouling properties. We next investigated the cell attachment on the P(qTR-CB) hydrogel in vitro. Hydrogels that resist cell attachment are desirable for many biomedical applications. For comparison, PHEMA, PCB hydrogels, and tissue culture polystyrene (TCPS) were used as controls. Fig. 2B showed that cells quickly attached, proliferated, and formed a confluent layer on the TCPS surfaces while there were almost no cells observed on the P(qTR-CB), PHEMA,

and PCB hydrogel surfaces, suggesting that P(qTR-CB) hydrogel behaved similarly to PHEMA and PCB.

We then studied macrophage activation on the P(qTR-CB) hydrogels by seeding murine bone marrow derived macrophages (BMDM). Macrophages as a key component of the FBR regulate pro-inflammatory or pro-healing processes [46]. Pro-inflammatory macrophages secrete inflammatory cytokines such as tumor necrosis factor- $\alpha$  (TNF- $\alpha$ ) that triggers further recruitment and activation of inflammatory cells, while pro-healing macrophages produce anti-inflammatory cytokines such as interleukin (IL-10) that facilitates angiogenesis and tissue repair. Understanding how a biomaterial regulates macrophage phenotype is thus of great importance for many biomedical applications. As shown in Fig. 2C and Fig. 2D, the levels of TNF-α and IL-10 secretion were almost undetectable for all the hydrogels without stimulation. With the stimulation of lipopolysaccharide/Interferon gamma (LPS/IFNy) which was known to induce a pro-inflammatory macrophage phenotype, the cells on the PCB and P(qTR-CB) hydrogels (Fig. 2C) secreted lower levels of TNF-α when compared to those cultured on the PHEMA hydrogel or the TCPS. With the stimulation of LPS/IL-4/IL-13 which was known to promote a pro-healing macrophage phenotype, the cells on PCB and P(qTR-CB) hydrogels (Fig. 2D) had an enhanced IL-10 secretion when compared to those on the PHEMA hydrogel. Taken together, these results showed that P(qTR-CB) hydrogels inhibited inflammatory activation and promoted pro-healing macrophage phenotype.

## 3.3. Design and mechanical characterization of the P(TR-CB) and P(TR-SB) hydrogels

Encouraged by the results we obtained from the P(qTR-CB), we designed two more triazole-containing zwitterionic monomers (TR-CB and TR-SB; Fig. 3A). The synthetic routes for the TR-CB and TR-SB monomers were shown, and their chemical structures were confirmed by

NMR in Supporting Information. Compared to the qTR-CB in which the triazole moiety was quaternized, the TR-CB and TR-SB monomers have an original, un-modified triazole group. The mechanical properties of the P(TR-CB) and P(TR-SB) hydrogels were evaluated. Similar to P(qTR-CB) hydrogels, the P(TR-CB) and P(TR-SB) hydrogels could endure repeated folding. Both hydrogels were highly resilient (Fig. 3B-D), especially the P(TR-SB) hydrogel (Fig. 3B-C, and Supplementary Movie 2), for which the maximum tensile strain was as high as 250%. By contrast, the maximum tensile strain for pure zwitterionic hydrogels reported to date was only 65% [42]. This is a drastic improvement in the field of zwitterionic hydrogels. When compared to PCB hydrogel, the breaking strains of P(TR-CB) and P(TR-SB) hydrogels were 9-fold and 20fold higher, respectively. It should be also noted that P(TR-CB) and P(TR-SB) hydrogels were more elastic than the P(qTR-CB). This may be attributed to the position of the positive charge on the qTR-CB triazole ring. The electrostatic repulsion between the charges may attenuate the  $\pi$ - $\pi$ stacking interaction. For compressive tests (Fig. 3D), both the P(TR-CB) and P(TR-SB) hydrogels had high compressive strains (79% and 89%, respectively). To the best of our knowledge, these TR-ZW hydrogels represent a first class of pure zwitterionic hydrogels with such robust mechanical properties. We also studied the internal morphology of freeze-dried TR-ZW hydrogel networks using a scanning electron microscope (SEM). Both P(qTR-CB) (Supplementary Fig. 1) and P(TR-CB) (Fig. 3E) hydrogels were highly porous after drying with a similar pore-size range of approximately 30 to 150 microns.

## 3.4. In vivo biocompatibility of the TR-ZW hydrogels

To investigate whether these new TR-ZW hydrogels (P(qTR-CB), P(TR-CB), and P(TR-SB)) had FBR-resistant properties, we implanted them subcutaneously in immunocompetent C57BL/6 mice. To date, the FBR is still a major concern for the performance and longevity of implanted

materials and devices. There is a critical need for development of novel hydrogel materials that both mitigate FBR and are mechanically robust. In this work, we evaluated the FBR to the implants at selected time points post implantation (1, 2, and 3 months). A commonly used biocompatible PHEMA hydrogel was chosen as control. At each time point, we retrieved the hydrogel samples and examined the FBR including the fibrosis around the implants using Masson's trichrome staining as well as the blood vessel formation using CD31 staining. At 1 month, we observed that all the TR-ZW hydrogels had loose collagen layers around them as indicated by the light blue color (Fig. 4A), while the PHEMA hydrogels had a much denser collagen deposition. The P(TR-SB) hydrogel had a particuarly low density of collagen deposition. Moreover, these TR-ZW hydrogels during retrieval appeared transparent, suggesting that collagen dopostion around them was thin or loose (Supplementary Fig. 2) compared to that around the PHEMA hydrogels which were more translucent. Although the presence of any collagen is indicative of the formation of a fibrotic capsule, loose collagen deposition is generally thought to have less impact on mass transfer [20]. Longer-term implantation experiments (i.e. 2 and 3 months) revealed similar results. The collagen density at the interface between the TR-ZW hydrogels and tissues was significantly lower when compared to the case of PHEMA control (Fig. 4B). To evaluate whether the stiffness of TR-ZW hydrogels had an impact on FBR, the Young's moduli of these hydrogels were measured (Supplementary Fig. 3). Among the three different TR-ZW hydrogels, P(TR-SB) which had lowest stiffness showed less collagen deposition than P(TR-CB) and P(qTR-CB) hydrogels. The results seem to suggest that smaller hydrogel modulus correlates with lower level of FBR, in agreement with previous work [47, 48].

It is also interesting to note that abundant blood vessels were observed around the TR-ZW hydrogels compared with the PHEMA hydrogel, especially for the 2 and 3 month implantations.

To better analyze the blood vessel formation, we stained the histological sections with an endothelial cell biomarker CD31 antibody. As shown in Fig. 4C-D, the blood-vessel density on the TR-ZW hydrogels was substantially higher than that of the PHEMA hydrogel. Among the different TR-ZW hydrogels, it was also found that the P(TR-SB) promoted even more blood vessel formation than the P(qTR-CB) after 2-month implantation. All these data together suggested that the TR-ZW hydrogels mitigated FBR in mice (i.e. induced less fibrosis and promoted more blood vessel formation).

When comparing the TR-ZW hydrogels with the previously reported PCB [20], we found that the density of collagen deposition and the number of blood vessels for the TR-ZW hydrogels were comparable to those for the PCB[20] (Supplementary Fig. 4). It is generally held that the antifouling properties or biocompatibility is compromised if hydrophobic moiety is incorporated into zwitterionic materials. The triazole group as a hydrophobic moiety indeed affected its antifouling properties. For example, the amount of plasma adsorption for P(qTR-CB), P(TR-CB), and P(TR-SB) surfaces was  $3.1 \pm 1.8$ ,  $6.4 \pm 2.5$ , and  $10.9 \pm 3.2$  ng/cm<sup>2</sup>, respectively (Supplementary Table 1) while PCB surface was reported to only adsorb <0.3 ng/cm<sup>2</sup> protein from plasma [45, 49]. However, the *in vivo* biocompatibility or the FBR-mitigating property of the TR-ZW hydrogels was not significantly affected. The triazole group might play a role here in mitigating the fibrotic response in addition to the zwitterionic moiety. Chemically modified alginates containing triazole groups were reported to be capable of mitigating the fibrotic response effectively [27]. The FBR-resistent property of the TR-ZW hydrogels was also consistent with the macrophage activation data (Figure 2C-D). However, more work is needed to elucidate the exact mechanisms in the future. More importantly, the combination of mechanical

robustness and FBR-mitigating properties for pure zwitterionic hydrogels has not been achieved before.

### 3.5. Diabetes Treatments in Mice

To demonstrate the applications of these FBR-mitigating and mechanically robust TR-ZW hydrogels, we tested the P(TR-SB) hydrogel for islet encapsulation for potential treatment of type 1 diabetes (T1D). T1D is an autoimmune disease where the patients' insulin-producing pancreatic islet cells are mistakenly destroyed by their own immune system. Islet encapsulation has been shown to be promising to treat T1D without immunosuppression [50-53]. However, one of the major obstacles is the FBR-caused fibrosis and lack of sufficient blood vessels around the encapsulation material, resulting in hypoxic condition and deficient mass transfer of nutrients, insulin and metabolic wastes [50]. We hypothesized the low level of fibrosis and high degree of vascularization of the robust P(TR-SB) hydrogel would improve the outcome of islet encapsulation (Fig. 5A). To test this hypothesis, we encapsulated rat islets in P(TR-SB) hydrogel disks and transplanted them subcutaneously in streptozotocin (STZ)-induced diabetic, C57BL/6 mice. Each of the mice received 1 disk (diameter: 6.5 mm; thickness: 1 mm) containing about ~500 islet equivalents isolated from rats (Fig. 5B). The encapsulated islets in P(TR-SB) hydrogel showed high viability post-gelation (Supplementary Fig. 5). A commonly used cell encapsulation material, alginate (ultrapure, sterile SLG100) was fabricated into disks with similar dimensions and number of islets, which were implanted as control. Shortly after transplantation, the blood glucose (BG) level of all the diabetic mice decreased to the normal glycemic range (BG < 200 mg/dL) (Fig. 5C). However, all the mice in the alginate control group gradually became diabetic again by day 18, indicating the failure of the devices. In contrast, 8 out of the 12 mice from the P(TR-SB) group remained normoglycemic for 1 month when the implants were retrieved. The BG of the cured mice went up after retrieval, confirming the function of the implants. An intraperitoneal glucose tolerance test (IPGTT) (Fig. 5D) was conducted on day 28 after transplantation. The mice in the P(TR-SB) group cleared blood glucose and restored normoglycemia at a rate comparable to that of non-diabetic mice within 90 min, further confirming the function of transplanted islets whereas the BG of the diabetic mice failed to drop to normal range even after 120 min. Furthermore, the glucose-stimulated insulin secretion (GSIS) assay performed on the retrieved P(TR-SB) hydrogels (Fig. 5E) suggested that encapsulated islets were responsive to glucose change and secreted insulin, indicating the viability and normal function of retrieved islets.

Post-retrieval characterizations showed that a number of visible blood vessels (Fig. 5F and Supplementary Fig. 6) were formed on the P(TR-SB) hydrogels encapsulating islets from the normoglycemic mouse group after 30 days of subcutaneous implantation. The histological analysis confirmed abundant vessels within loose fibrotic layers around the devices (Fig. 5G-H, and Supplementary Fig. 6). Interestingly, we observed fewer vessels around the islet/hydrogel constructs from mice that experienced earlier failure of transplantation (Supplementary Fig. 6). There seemed to be a positive correlation between the transplantation outcome and the level of vascularization. As control, Alginate hydrogels (Supplementary Fig. 7) were found to induce denser collagen deposition and a lower degree of vascularization compared to zwitterionic hydrogels. To further investigate whether generated vessels were functionally connected to host vasculature, we perfused mice implanted with the P(TR-SB) hydrogel through cardiac injection of lipophilic carbocyanine dye DiI that was widely used to stain blood vessels [38]. The result of blood vessel perfusion (Fig. 5I) confirmed that P(TR-SB) hydrogel-induced vessels were

functional. The islets in the retrieved P(TR-SB) hydrogels shrank in size indicating sub-optimal survival conditions within the hydrogel in the subcutaneous space. However, they were still functional, as verified by H&E histological analysis (Fig. 5J) and positive insulin staining (Fig. 5K). Taken together, these above data provide a proof of concept for the potential use of the TR-ZW hydrogels for islet encapsulation.

### 4. Conclusion

In summary, we have designed and synthesized a new class of triazole-zwitterionic hydrogels that were mechanically robust and exhibited FBR-mitigating effect in mice. Compared to conventional zwitterionic hydrogels which are typically weak or brittle, these novel TR-ZW hydrogels were more resilent with higher stretchability, better compression-resistance and better folding-resistance. These hydrogels retained antifouling characteristics, expected for zwitterionic materials. More importantly, the robust TR-ZW hydrogels mitigated the fibrosis and promoted the blood vessel formation compared with other common hydrogels such as PHEMA. These robust and biocompatible hydrogels are desirable for many biomedical applications particularly the islet encapsulation where durable mechanical stability with suitable stiffness, mild fibrosis with low collagen density and high vascularization with close proximity to islets are all beneficial. Using a rat-to-mouse transplantation model, we demonstrated that the P(TR-SB) hydrogel despite variations induced a less dense fibrotic layer and more vessels within the fibrotic layer than alginate and improved diabetes correction through a convenient subcutaneous implantation.

## Acknowledgments

This research was partially supported by the Juvenile Diabetes Research Foundation (JDRF), the Hartwell Foundation, the National Institutes of Health (NIH, 1R01DK105967-01A1) and the Novo Nordisk Company. SEM measurements performed in this work made use of the Cornell Center for Materials (CCMR) Research Shared Facilities which are supported through the NSF MRSEC program (DMR-1719875).

### **Author contributions**

Q.L. and M.M. conceived and designed the project. A.C. and D.A. performed *in vivo* experiments in mouse and analyzed the samples. L.W., Y.Z., S.M., Y.P. and J. C. performed immunohistochemical experiments and helped to analyze data. W.L. and L.L. performed protein adsorption studies. E.C. and W.L. performed macrophage activation studies. All authors reviewed the manuscript and provided input.

### **Conflict of Interest**

The authors declare no competing financial interests.

# **Supporting Information**

All data associated with this study are present in the paper or the Supporting Information.

### References

- [1] R. Mahou, A.E. Vlahos, A. Shulman, M.V. Sefton, Interpenetrating Alginate-Collagen Polymer Network Microspheres for Modular Tissue Engineering, ACS Biomaterials Science & Engineering 4(11) (2017) 3704-3712.
- [2] N.A. Peppas, J.Z. Hilt, A. Khademhosseini, R. Langer, Hydrogels in biology and medicine: from molecular principles to bionanotechnology, Advanced materials 18(11) (2006) 1345-1360.
- [3] J. Zhang, Y. Zhu, J. Song, T. Xu, J. Yang, Y. Du, L. Zhang, Rapid and Long Term Glycemic Regulation with a Balanced Charged Immune Evasive Hydrogel in T1DM Mice, Advanced Functional Materials (2019) 1900140.
- [4] D. An, Y. Ji, A. Chiu, Y.-C. Lu, W. Song, L. Zhai, L. Qi, D. Luo, M. Ma, Developing robust, hydrogel-based, nanofiber-enabled encapsulation devices (NEEDs) for cell therapies, Biomaterials 37 (2015) 40-48.

- [5] D.M. Headen, G. Aubry, H. Lu, A.J. García, Microfluidic based generation of size controlled, biofunctionalized synthetic polymer microgels for cell encapsulation, Advanced materials 26(19) (2014) 3003-3008.
- [6] D.W. Grainger, All charged up about implanted biomaterials: a zwitterionic polymer hinders the foreign-body response that leads to fibrotic encapsulation of implants, Nature biotechnology 31(6) (2013) 507-510.
- [7] M.D. Swartzlander, C.A. Barnes, A.K. Blakney, J.L. Kaar, T.R. Kyriakides, S.J. Bryant, Linking the foreign body response and protein adsorption to PEG-based hydrogels using proteomics, Biomaterials 41 (2015) 26-36.
- [8] T.T. Lee, J.R. García, J.I. Paez, A. Singh, E.A. Phelps, S. Weis, Z. Shafiq, A. Shekaran, A. Del Campo, A.J. García, Light-triggered in vivo activation of adhesive peptides regulates cell adhesion, inflammation and vascularization of biomaterials, Nature materials 14(3) (2015) 352-360.
- [9] A.D. Lynn, T.R. Kyriakides, S.J. Bryant, Characterization of the in vitro macrophage response and in vivo host response to poly (ethylene glycol) based hydrogels, Journal of Biomedical Materials Research Part A 93(3) (2010) 941-953.
- [10] S. Sharma, R.W. Johnson, T.A. Desai, Evaluation of the stability of nonfouling ultrathin poly (ethylene glycol) films for silicon-based microdevices, Langmuir 20(2) (2004) 348-356.
- [11] O. Veiseh, J.C. Doloff, M. Ma, A.J. Vegas, H.H. Tam, A.R. Bader, J. Li, E. Langan, J. Wyckoff, W.S. Loo, Size-and shape-dependent foreign body immune response to materials implanted in rodents and non-human primates, Nature materials 14(6) (2015) 643-651.
- [12] J. Zhang, Y. Zhu, J. Song, J. Yang, C. Pan, T. Xu, L. Zhang, Novel Balanced Charged Alginate/PEI Polyelectrolyte Hydrogel that Resists Foreign-Body Reaction, ACS applied materials & interfaces 10(8) (2018) 6879-6886.
- [13] W. Yang, H. Xue, W. Li, J. Zhang, S. Jiang, Pursuing "zero" protein adsorption of poly (carboxybetaine) from undiluted blood serum and plasma, Langmuir 25(19) (2009) 11911-11916.
- [14] R. Yang, J. Xu, G. Ozaydin-Ince, S.Y. Wong, K.K. Gleason, Surface-tethered zwitterionic ultrathin antifouling coatings on reverse osmosis membranes by initiated chemical vapor deposition, Chemistry of Materials 23(5) (2011) 1263-1272.
- [15] Y. Zhu, J. Wang, F. Zhang, S. Gao, A. Wang, W. Fang, J. Jin, Zwitterionic Nanohydrogel Grafted PVDF Membranes with Comprehensive Antifouling Property and Superior Cycle Stability for Oil in Water Emulsion Separation, Advanced Functional Materials 28(40) (2018) 1804121.
- [16] T. Shimizu, T. Goda, N. Minoura, M. Takai, K. Ishihara, Super-hydrophilic silicone hydrogels with interpenetrating poly (2-methacryloyloxyethyl phosphorylcholine) networks, Biomaterials 31(12) (2010) 3274-3280.
- [17] Y. Wen, Z. Zhang, J. Li, Highly Efficient Multifunctional Supramolecular Gene Carrier System Self Assembled from Redox Sensitive and Zwitterionic Polymer Blocks, Advanced Functional Materials 24(25) (2014) 3874-3884.
- [18] J. Park, J. Nam, N. Won, H. Jin, S. Jung, S. Jung, S.H. Cho, S. Kim, Compact and stable quantum dots with positive, negative, or zwitterionic surface: specific cell interactions and non specific adsorptions by the surface charges, Advanced Functional Materials 21(9) (2011) 1558-1566.
- [19] T. Mizuhara, K. Saha, D.F. Moyano, C.S. Kim, B. Yan, Y.K. Kim, V.M. Rotello, Acylsulfonamide Functionalized Zwitterionic Gold Nanoparticles for Enhanced Cellular Uptake at Tumor pH, Angewandte Chemie International Edition 54(22) (2015) 6567-6570.

- [20] L. Zhang, Z. Cao, T. Bai, L. Carr, J.-R. Ella-Menye, C. Irvin, B.D. Ratner, S. Jiang, Zwitterionic hydrogels implanted in mice resist the foreign-body reaction, Nature biotechnology 31(6) (2013) 553.
- [21] A. Azvolinsky, C. Schmidt, E. Waltz, S. Webb, 20 years of Nature Biotechnology biomedical research, Nature 201 (2016) 6.
- [22] B. Cao, Q. Tang, L. Li, J. Humble, H. Wu, L. Liu, G. Cheng, Switchable antimicrobial and antifouling hydrogels with enhanced mechanical properties, Advanced healthcare materials 2(8) (2013) 1096-1102.
- [23] L.R. Carr, Y. Zhou, J.E. Krause, H. Xue, S. Jiang, Uniform zwitterionic polymer hydrogels with a nonfouling and functionalizable crosslinker using photopolymerization, Biomaterials 32(29) (2011) 6893-6899.
- [24] N.Y. Kostina, C. Rodriguez-Emmenegger, M. Houska, E. Brynda, J.í. Michálek, Nonfouling hydrogels of 2-hydroxyethyl methacrylate and zwitterionic carboxybetaine (meth) acrylamides, Biomacromolecules 13(12) (2012) 4164-4170.
- [25] J. Ning, G. Li, K. Haraguchi, Synthesis of highly stretchable, mechanically tough, zwitterionic sulfobetaine nanocomposite gels with controlled thermosensitivities, Macromolecules 46(13) (2013) 5317-5328.
- [26] N.Y. Kostina, S. Sharifi, A. de los Santos Pereira, J. Michálek, D.W. Grijpma, C. Rodriguez-Emmenegger, Novel antifouling self-healing poly (carboxybetaine methacrylamide-co-HEMA) nanocomposite hydrogels with superior mechanical properties, Journal of Materials Chemistry B 1(41) (2013) 5644-5650.
- [27] A.J. Vegas, O. Veiseh, J.C. Doloff, M. Ma, H.H. Tam, K. Bratlie, J. Li, A.R. Bader, E. Langan, K. Olejnik, Combinatorial hydrogel library enables identification of materials that mitigate the foreign body response in primates, Nature biotechnology 34(3) (2016) 345-352.
- [28] M.A. Bochenek, O. Veiseh, A.J. Vegas, J.J. McGarrigle, M. Qi, E. Marchese, M. Omami, J.C. Doloff, J. Mendoza-Elias, M. Nourmohammadzadeh, Alginate encapsulation as long-term immune protection of allogeneic pancreatic islet cells transplanted into the omental bursa of macaques, Nature biomedical engineering 2(11) (2018) 810.
- [29] L. Latxague, M.A. Ramin, A. Appavoo, P. Berto, M. Maisani, C. Ehret, O. Chassande, P. Barthélémy, Control of Stem Cell Behavior by Fine Tuning the Supramolecular Assemblies of Low Molecular Weight Gelators, Angewandte Chemie International Edition 54(15) (2015) 4517-4521.
- [30] S.-H. Jung, J. Ryu, D. Sohn, H.-i. Lee, Time-dependent increase in aqueous solubility caused by the gradual disruption of hydrophobic aggregation, Polymer Chemistry 3(4) (2012) 1002-1006.
- [31] T.L. Sun, T. Kurokawa, S. Kuroda, A.B. Ihsan, T. Akasaki, K. Sato, M.A. Haque, T. Nakajima, J.P. Gong, Physical hydrogels composed of polyampholytes demonstrate high toughness and viscoelasticity, Nature materials 12(10) (2013) 932-937.
- [32] Z. Zhang, S. Chen, S. Jiang, Dual-functional biomimetic materials: nonfouling poly (carboxybetaine) with active functional groups for protein immobilization, Biomacromolecules 7(12) (2006) 3311-3315.
- [33] P. Zhang, F. Sun, C. Tsao, S. Liu, P. Jain, A. Sinclair, H.-C. Hung, T. Bai, K. Wu, S. Jiang, Zwitterionic gel encapsulation promotes protein stability, enhances pharmacokinetics, and reduces immunogenicity, Proceedings of the National Academy of Sciences 112(39) (2015) 12046-12051.

- [34] J.E. Krause, N.D. Brault, Y. Li, H. Xue, Y. Zhou, S. Jiang, Photoiniferter-Mediated Polymerization of Zwitterionic Carboxybetaine Monomers for Low-Fouling and Functionalizable Surface Coatings, Macromolecules 44(23) (2011) 9213-9220.
- [35] P. Morgado, Y.-C. Ong, J.C. Boothroyd, M.B. Lodoen, Toxoplasma gondii induces B7-2 expression through activation of JNK signal transduction, Infection and immunity 79(11) (2011) 4401-4412.
- [36] P.E. Lacy, M. Kostianovsky, Method for the isolation of intact islets of Langerhans from the rat pancreas, Diabetes 16(1) (1967) 35-39.
- [37] C. Ricordi, D.W. Gray, B.J. Hering, D.B. Kaufman, G.L. Warnock, N.M. Kneteman, S.P. Lake, N.J. London, C. Socci, R. Alejandro, Islet isolation assessment in man and large animals, Acta diabetologia latina 27(3) (1990) 185-195.
- [38] Y. Li, Y. Song, L. Zhao, G. Gaidosh, A.M. Laties, R. Wen, Direct labeling and visualization of blood vessels with lipophilic carbocyanine dye DiI, Nature protocols 3(11) (2008) 1703.
- [39] S.K. Seth, V.S. Lee, J. Yana, S.M. Zain, A.C. Cunha, V.F. Ferreira, A.K. Jordão, M.C. de Souza, S.M. Wardell, J.L. Wardell, Crystallographic and computational study of 1-(arylamino)-1, 2, 3-triazole-4-carbohydrazides, CrystEngComm 17(11) (2015) 2255-2266.
- [40] P. Kočalka, N.K. Andersen, F. Jensen, P. Nielsen, Synthesis of 5 (1, 2, 3 Triazol 4
- yl) 2' deoxyuridines by a Click Chemistry Approach: Stacking of Triazoles in the Major Groove Gives Increased Nucleic Acid Duplex Stability, ChemBioChem 8(17) (2007) 2106-2116.
- [41] Z. Zhang, T. Chao, S. Jiang, Physical, chemical, and chemical—physical double network of zwitterionic hydrogels, The Journal of Physical Chemistry B 112(17) (2008) 5327-5332.
- [42] B. Cao, L. Li, Q. Tang, G. Cheng, The impact of structure on elasticity, switchability, stability and functionality of an all-in-one carboxybetaine elastomer, Biomaterials 34(31) (2013) 7592-7600.
- [43] M.C. Darnell, J.-Y. Sun, M. Mehta, C. Johnson, P.R. Arany, Z. Suo, D.J. Mooney, Performance and biocompatibility of extremely tough alginate/polyacrylamide hydrogels, Biomaterials 34(33) (2013) 8042-8048.
- [44] S.Y. Son, J.-H. Kim, E. Song, K. Choi, J. Lee, K. Cho, T.-S. Kim, T. Park, Exploiting  $\pi$ – $\pi$  stacking for stretchable semiconducting polymers, Macromolecules 51(7) (2018) 2572-2579.
- [45] S. Jiang, Z. Cao, Ultralow fouling, functionalizable, and hydrolyzable zwitterionic materials and their derivatives for biological applications, Advanced materials 22(9) (2010) 920-932.
- [46] E.Y. Chen, S. Chu, L. Gov, Y.K. Kim, M.B. Lodoen, A.J. Tenner, W.F. Liu, CD200 modulates macrophage cytokine secretion and phagocytosis in response to poly (lactic coglycolic acid) microparticles and films, Journal of Materials Chemistry B (2017).
- [47] L.E. Jansen, L.D. Amer, E.Y.-T. Chen, T.V. Nguyen, L.S. Saleh, T. Emrick, W.F. Liu, S.J. Bryant, S.R. Peyton, Zwitterionic PEG-PC hydrogels modulate the foreign body response in a modulus-dependent manner, Biomacromolecules 19(7) (2018) 2880-2888.
- [48] A.K. Blakney, M.D. Swartzlander, S.J. Bryant, The effects of substrate stiffness on the in vitro activation of macrophages and in vivo host response to poly (ethylene glycol)-based hydrogels, Journal of biomedical materials research. Part A 100(6) (2012) 1375.
- [49] J. Ladd, Z. Zhang, S. Chen, J.C. Hower, S. Jiang, Zwitterionic polymers exhibiting high resistance to nonspecific protein adsorption from human serum and plasma, Biomacromolecules 9(5) (2008) 1357-1361.
- [50] D. An, A. Chiu, J.A. Flanders, W. Song, D. Shou, Y.-C. Lu, L.G. Grunnet, L. Winkel, C. Ingvorsen, N.S. Christophersen, Designing a retrievable and scalable cell encapsulation device

for potential treatment of type 1 diabetes, Proceedings of the National Academy of Sciences 115(2) (2018) E263-E272.

- [51] R. Mahou, D.K. Zhang, A.E. Vlahos, M.V. Sefton, Injectable and inherently vascularizing semi-interpenetrating polymer network for delivering cells to the subcutaneous space, Biomaterials 131 (2017) 27-35.
- [52] T. Desai, L.D. Shea, Advances in islet encapsulation technologies, Nature reviews Drug discovery 16(5) (2017) 338.
- [53] A.A. Tomei, V. Manzoli, C.A. Fraker, J. Giraldo, D. Velluto, M. Najjar, A. Pileggi, R.D. Molano, C. Ricordi, C.L. Stabler, Device design and materials optimization of conformal coating for islets of Langerhans, Proceedings of the National Academy of Sciences 111(29) (2014) 10514-10519.

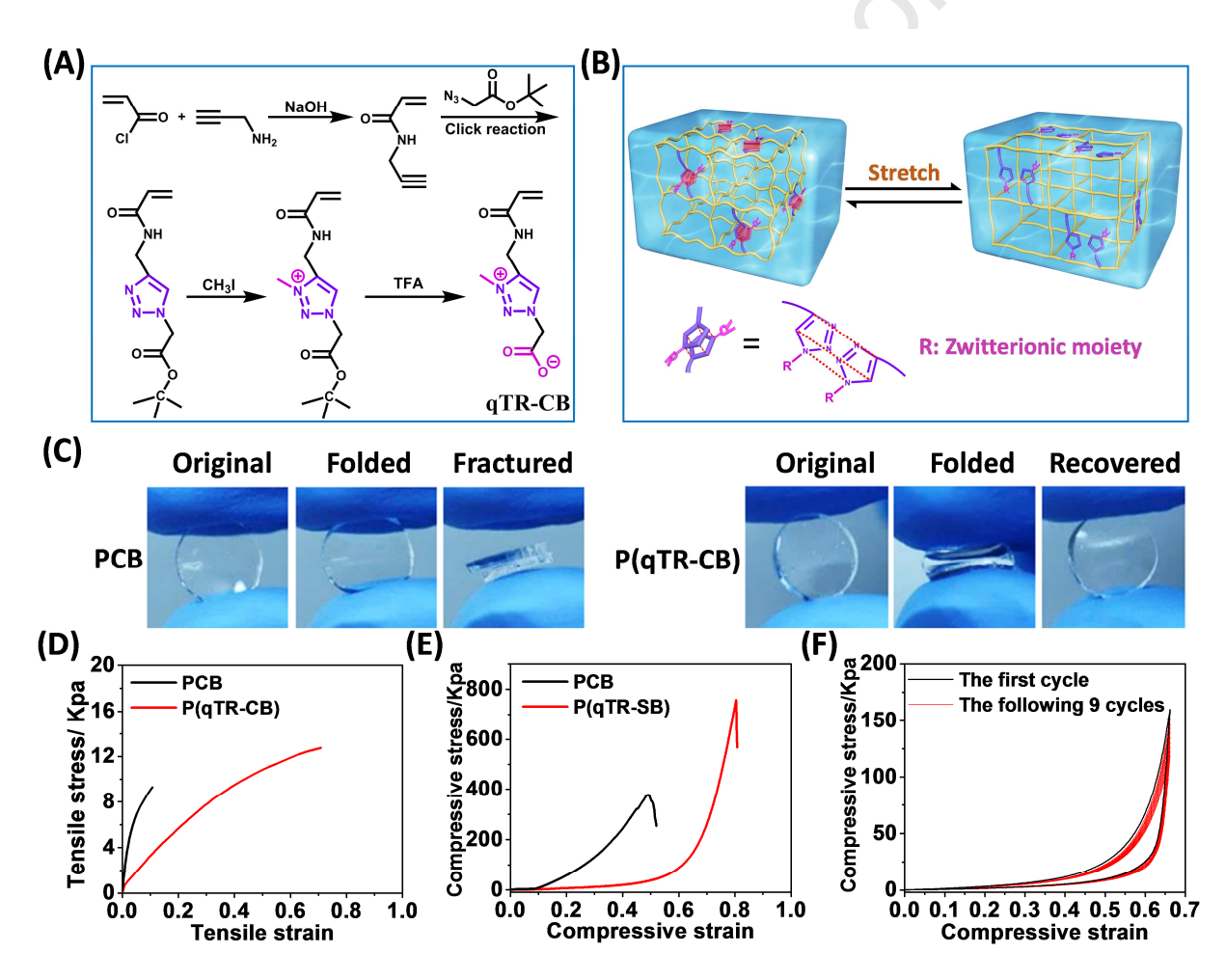
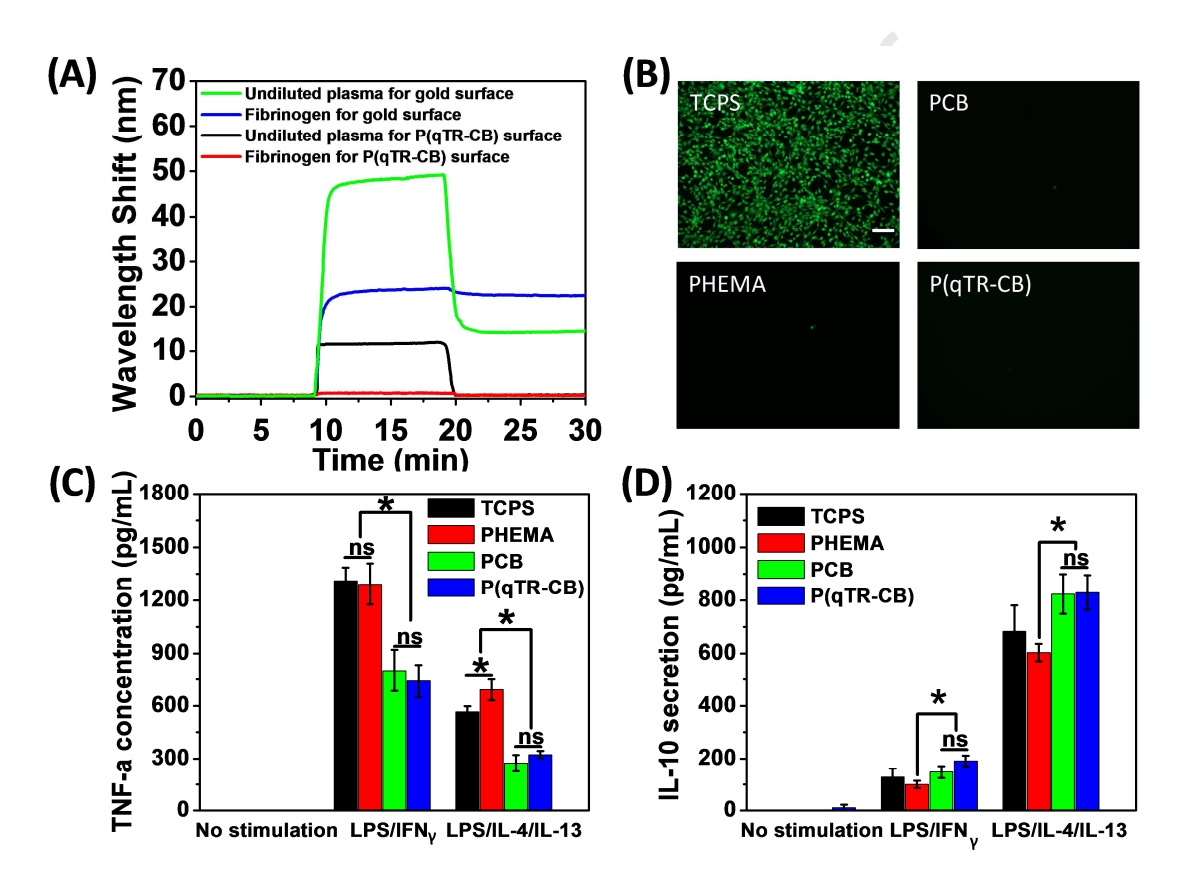
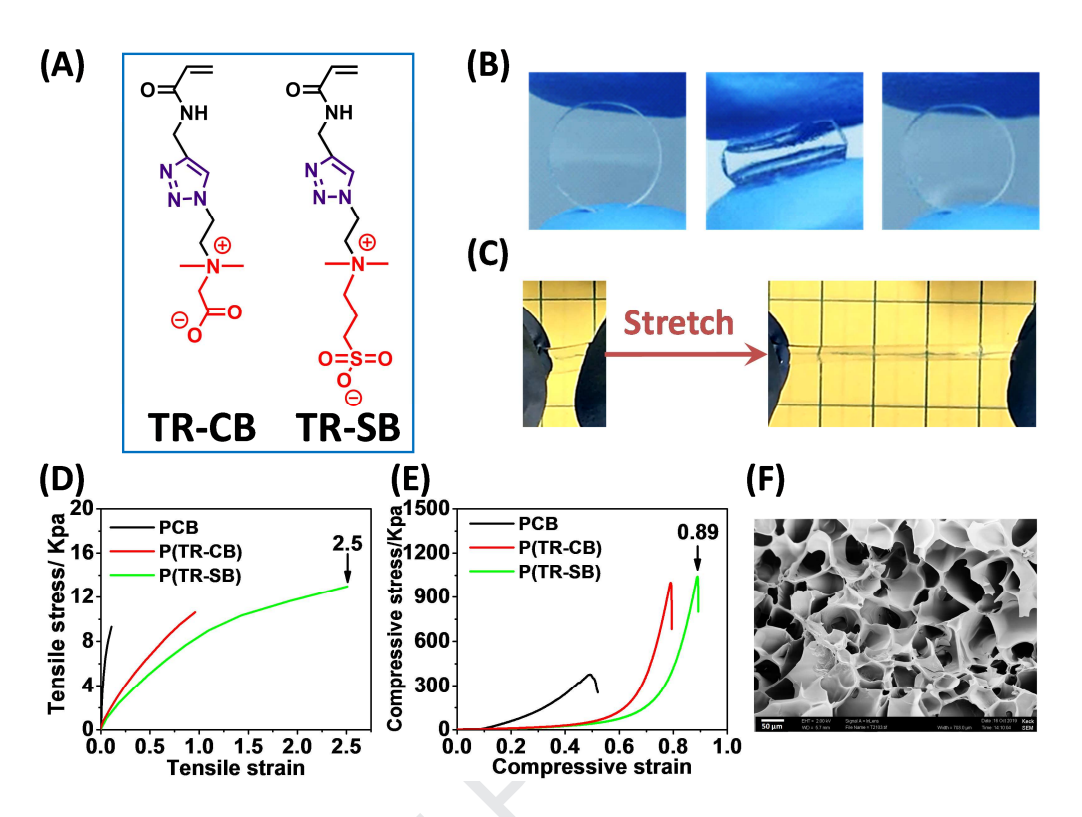


Fig 1. Synthesis of the qTR-CB monomer, and characterization of mechanical properties of the P(qTR-CB) hydrogel. (A) Synthetic route of qTR-CB material. (B) A schematic illustration showing the  $\pi$ - $\pi$  stacking between the triazole rings as potential mechanism for energy dissipation. (C) Images of PCB and P(qTR-CB) hydrogels during folding test. (D) Stress-strain curves for PCB and P(qTR-CB) hydrogels

in tensile test. **(E)** Stress-strain curves for PCB and P(qTR-CB) hydrogels in compression test. **(F)** Stress-strain curves of ten consecutive loading-unloading cycles for the P(qTR-CB) hydrogel.



**Fig 2.** *In vitro* **characterization of the P(qTR-CB) hydrogel. (A)** Typical SPR sensorgrams showing protein adsorption from 1 mg/mL Fg or undiluted human plasma on the P(qTR-CB)-grafted or bare gold surfaces. **(B)** Fluorescent microscopic images of NIH/3T3 cells after 3-days of culturing on TCPS, PHEMA, PCB, and P(qTR-CB) hydrogel surfaces (Scale bars: 100 μm). **(C, D)** Quantification of (C) TNF- $\alpha$  and (D) IL10 secretion from macrophages cultured on various surfaces. (Mean ± SEM; n= 6; \*P < 0.05; ns, not significant).



**Fig 3. Synthesis of the TR-CB and TR-SB monomers and characterizations of mechanical properties of P(TR-CB) and P(TR-SB) hydrogels.** (A) Chemical structures of TR-CB and TR-SB monomers. (B) Images of P(TR-SB) hydrogels during folding test. (C) Stretching of a P(TR-SB) hydrogel. (D) Stress-strain curves for the PCB, P(TR-CB), and P(TR-SB) hydrogels in tensile test. (E) Stress-strain curves for the PCB, P(TR-CB), and P(TR-SB) hydrogels in compression test. (F) SEM image of freezedried P(TR-CB) hydrogel. Scale bar, 50 μm.

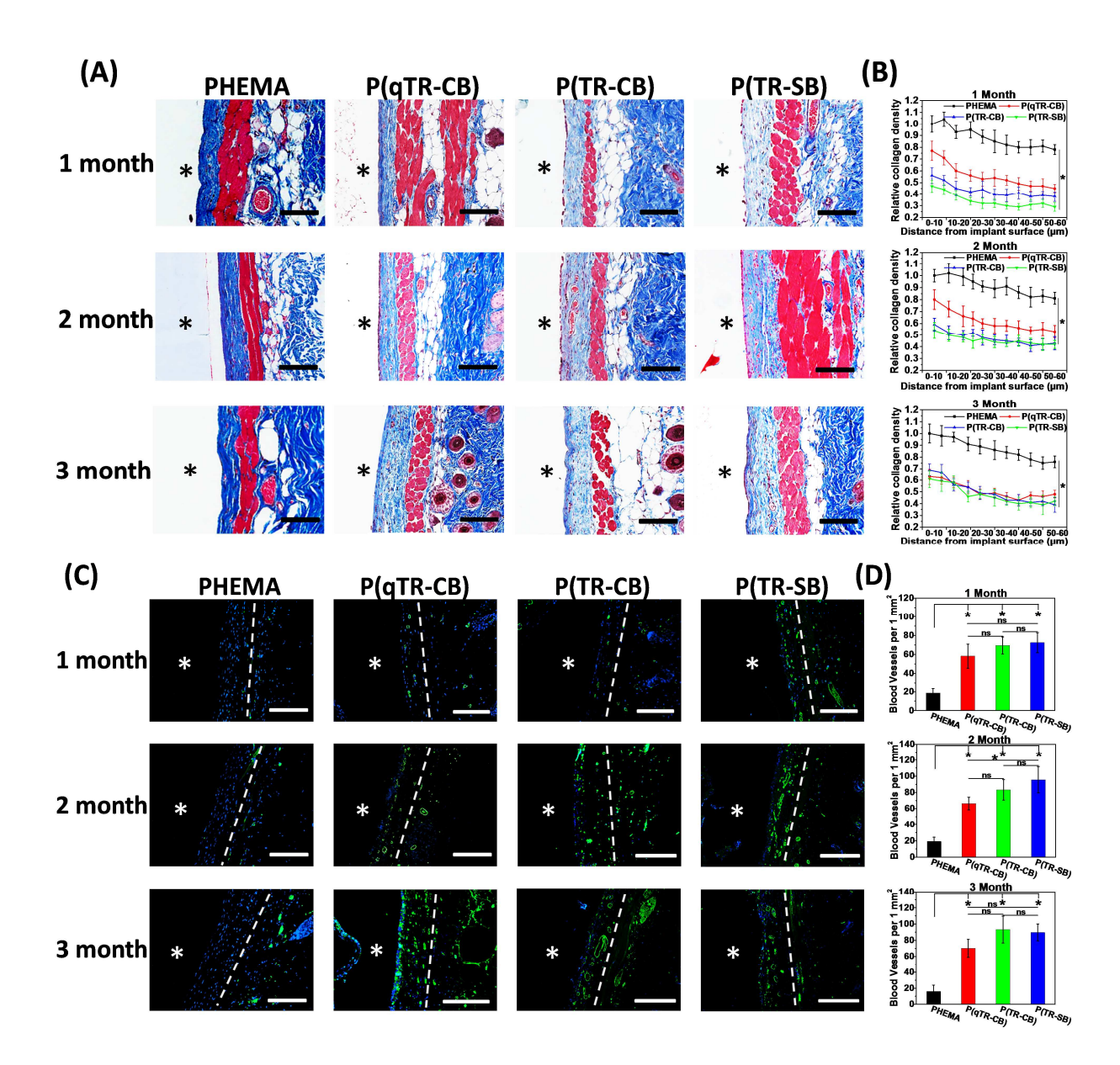


Fig 4. Characterization of FBR to various hydrogels in immunocompetent mice. (A) Representative Masson's trichrome staining images of different hydrogels retrieved at selected time points after subcutaneous implantation. The blue staining indicates fibrosis or collagen deposition surrounding implants (Scale bars: 100  $\mu$ m; asterisks indicate the location of the implanted hydrogel). (B) Quantification of collagen density around the implants (n=5). All data are presented as mean  $\pm$  SEM. \* $^{*}P$  < 0.05. (C) Representative CD31 immunostaining images. Blood vessels are stained dark green and nuclei are stained blue (Scale bars: 100  $\mu$ m; asterisks indicate the location of the implanted hydrogel and dashed lines indicate the border between the fibrotic layer and the skin tissue). (D) Quantification of blood vessel density around the implants (n=5). All data are presented as mean  $\pm$  SEM. \* $^{*}P$  < 0.05; ns, not significant.

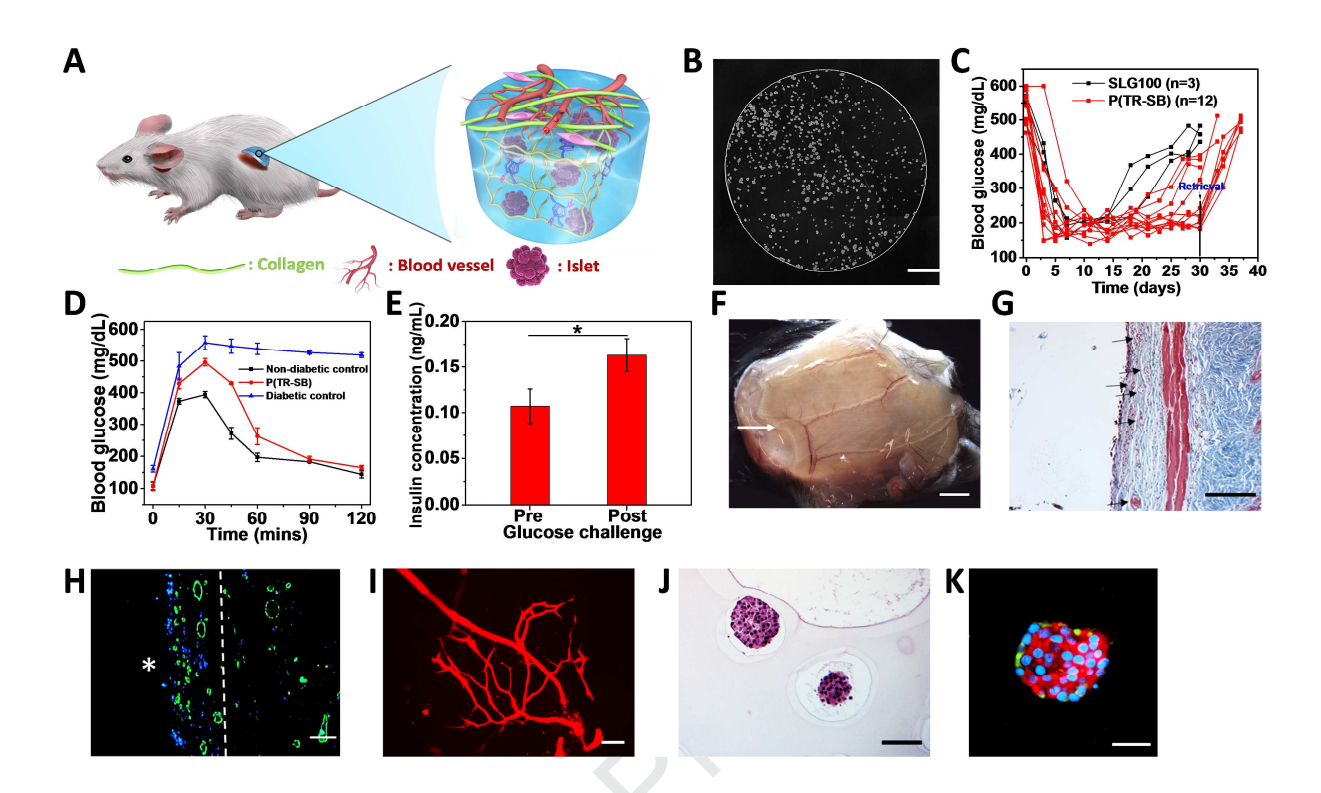


Fig 5. Islet encapsulation for potential diabetes treatment using triazole-zwitterionic hydrogels. (A) Schematic illustration of the low level of fibrosis and high degree of vascularization around the robust

P(TR-SB) hydrogel for islet encapsulation. (B) Macroscopic image of P(TR-SB) hydrogels encapsulating rat islets before implantation (Scale bar, 1 mm). (C) Blood glucose concentrations (n = 12 for P(TR-SB) hydrogels and n = 3 for SLG100 hydrogels, mean  $\pm$  SEM) of STZ-induced diabetic mice transplanted with encapsulated rat islets after 30 days of subcutaneous transplantation. (D) Intraperitoneal glucose tolerance test (IPGTT) before retrieval on day 28, n = 3 for each group, mean  $\pm$  SEM. (E) Ex vivo glucose stimulated insulin secretion (GSIS) of retrieved rat islets in P(TR-SB) hydrogels, n = 3, mean  $\pm$  SEM, \*P < 0.05. (F) Macroscopic image of P(TR-SB) hydrogels encapsulating rat islets after implantation (Scale bar, 1mm). Arrow points to an implanted hydrogel. (G) Representative Masson's trichrome staining image of retrieved P(TR-SB) hydrogels (Scale bar, 100 µm). Arrow indicates blood vessels. (H) Representative CD31 immunostaining image of retrieved P(TR-SB) hydrogels (Scale bar, 50 µm; green: blood vessels and blue: nuclei). Note: Asterisk indicates the location of the implanted hydrogel and dashed line indicates the border between the fibrotic layer and the skin tissue. (I) Confocal image of perfused blood vessels in the P(TR-SB) hydrogel (Scale bar, 100 µm). (J) An H&E stained crosssectional image of retrieved rat islets in P(TR-SB) hydrogels (Scale bar, 100 µm). (K) Immunohistochemical staining of rat islets in P(TR-SB) hydrogels (Scale bar, 100 µm; red: insulin, green: glucagon and blue: nuclei).

Journal President

### Journal Pre-proof

Declaration of interests
oxtimes The authors declare that they have no known competing financial interests or personal relationships that could have appeared to influence the work reported in this paper.
☐The authors declare the following financial interests/personal relationships which may be considered as potential competing interests: